

# AEROSOL DEPOSITION AND MOLD-FILLING METHOD FOR MICRO THERMOELECTRIC GENERATOR

N. Kouma\*, K. Hayashi, Y. Mizuno, O. Tsuboi, S. Sato and T. Iwai  
Energy Technology Lab., FUJITSU LABORATORIES LTD., Atsugi, Japan  
\*Presenting Author: kouma@jp.fujitsu.com

**Abstract:** To the best of our knowledge, we have succeeded in forming for the first time, thick thermoelectric ceramic structures of high-density and with a high-aspect-ratio, by using aerosol deposition (AD) and micromachined silicon molding. We achieved mold filling by controlling the kinetic energy of powder. Deposition conditions, I-V properties and thermal conductivities are examined, and the impact of integration on AD and micromachining process is described.

**Keywords:** aerosol deposition, silicon molding, thermoelectric generator, AZO

## INTRODUCTION

Micro thermoelectric generators ( $\mu$ TEGs) are becoming an important technology for energy harvesting, which converts waste thermal energy into electrical power, and for microscale power source applications in MEMS devices. Design studies suggest that the length of the thermoleg for vertical  $\mu$ TEGs should be optimized to obtain maximum output power because  $\mu$ TEGs having low thermal resistance are sensitive to thermal losses on the substrate supporting thermolegs [1]. The optimum length in many cases is between tens to hundreds of microns in which range it is hard to fabricate high-aspect-ratio thermolegs. With conventional thin film based micromachining technologies as well, it is difficult to deposit thick layers exceeding ten microns. Previously reported works fabricate  $\mu$ TEGs with high-aspect-ratio thermolegs by using various methods such as cosputtering [2], electroplating [1], inkjet to polymer mold [3] and a silicon molding process [4]. Active materials used in these works include V-VI compounds, which are known to be a good thermoelectric material for application at around room temperature.

Oxide thermoelectric materials are also good candidates for the energy conversion application due to their being non-toxic, low-cost and thermally stable [5]; however, they are not applied to micro thermoelectric generators. This seems to be due to the difficulty in shaping high-aspect-ratio structures and the necessity of high temperature treatment to form crystalline. Using the silicon molding process based on hot isostatic pressing (HIP) [6] is one effective solution for fabricating ceramic based microstructures; however, it is desirable to avoid high temperatures and high-pressure processes such as HIP for compatibility with semiconductor fabrication processes. We attempted to apply the aerosol deposition (AD) method for filling the micromachined mold.

The AD method is an attractive film formation method that uses powder collisions with a substrate [7]. Various films are obtained at low temperature and at a high deposition rate by selecting powders and

controlling their kinetic energy. The unique point of this method is that dense ceramic layers are formed at room temperature without binder. This method is thought to be suitable for mold filling. As a previous work for forming microstructures reports, the AD method is combined with a lift-off process [7]; however, with this method, it is difficult to obtain more than 100- $\mu$ m-thick fine patterns for the use of micro thermoelectric devices.

In this paper, we apply the AD method for filling the micromachined molding, with the aim of realizing fine patterns of thick ceramic layer with highly dense integration and a high-aspect-ratio. We evaluate the properties of fabricated ceramic structures for the use of thermoelectric materials.

## FABRICATION AND EXPERIMENT

Figure 1 shows a concept of the fabrication process. It consists of the following major steps: (a) micromachining a molding substrate; (b) mold-filling with the powder by using the AD method; (c) etching the molding.

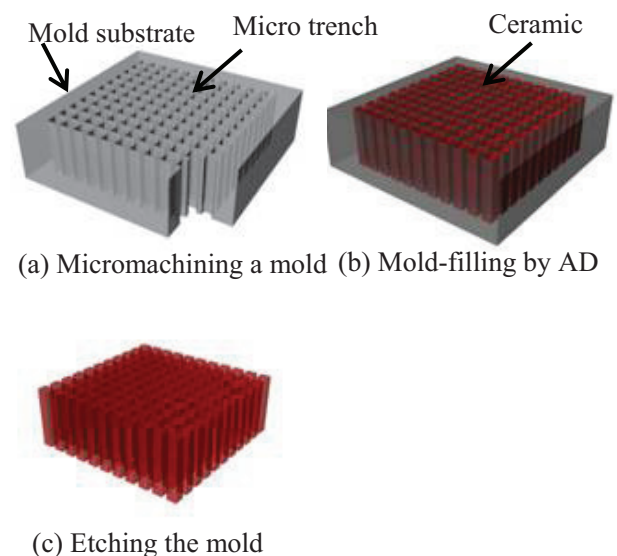


Fig. 1: A concept of fabrication process using a micromachined mold.

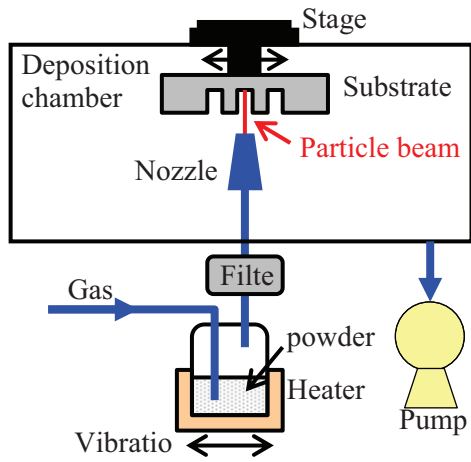


Fig. 2: Schematic diagram of the AD apparatus.

Table 1: Deposition condition with AD.

| Items                      | Conditions               |
|----------------------------|--------------------------|
| Powder                     | AZO                      |
| Primary powder size        | 3 $\mu\text{m}$ , 200 nm |
| Substrate                  | Si (SOI) wafer           |
| Carrier gas                | O <sub>2</sub>           |
| Size of nozzle orifice     | 5 x 0.3 mm <sup>2</sup>  |
| Scanning rate              | 300 mm/min               |
| Working pressure           | 150 Pa                   |
| Consumption of carrier gas | 9 L/min                  |
| Working distance           | 10 mm                    |
| Deposition temperature     | Room temperature         |

Figure 2 shows a schematic diagram of the AD apparatus. It consists of two vacuum chambers connected through a gas pipe. One is the deposition chamber and the other is the aerosol chamber. The deposition chamber contains a nozzle and substrate stage, and is vacuumed by a rotary pump and a mechanical booster pump. The aerosol chamber contains a heater, carrier gas introducing system and vibration system for powder mixing with the carrying gas. Ceramic powder contained in the aerosol chamber is delivered to the deposition chamber by the difference in pressure between the two chambers, and ejected through the micro orifice nozzle and deposited onto the substrate. Table 1 shows the AD conditions of the mold filling. Al-doped zinc oxide (AZO) powder is selected for the starting material. It is one of the most promising n-type TE oxides due to its attractive thermoelectric properties [8]; however, it is predicted that zinc oxide (ZnO) is one of the more difficult materials to obtain in thick layers with AD due to its breakdown behavior [9]. Thus, the micro molding process may be the only available method for shaping high-aspect-ratio structures of AZO. The primary sizes of the powders are about 200 nm and 3 $\mu\text{m}$ . The volume resistivity of the powder is about 100-500  $\Omega\text{cm}$ . The powders are heat treated at 350 degrees C before they are packed into the aerosol chamber.

Details of the process flow to fabricate microstructures are shown in Fig.3. An SOI (silicon on

insulator) wafer is used. Silicon is suitable for molding due to its high melting point, high hardness and ease of processing with anisotropic dry etching. Thicknesses of a handle layer and a BOX (buried oxide) layer are 60  $\mu\text{m}$  and 1  $\mu\text{m}$ , respectively. First, a surface of the handle layer is spin-coated with a positive photoresist film. After photolithography of the molding pattern, the handle layer is etched with deep reactive ion etching (DRIE) until the BOX layer is exposed. The silicon molding substrate with 60- $\mu\text{m}$ -depth patterns is completed after removing the photoresist. The obtained molding substrate is filled with AZO powders by AD. After the AZO layer deposited on the silicon surface is removed by wet etching, the silicon molding is selectively removed by dry etching of SF<sub>6</sub> plasma. By using above-mentioned process, AZO microstructures are achieved on the BOX layer.

It is not easy to evaluate the characteristics of a microstructure; thus, a different shape is formed according to the evaluation item as shown in Fig. 4. Figure 4(a) shows a test structure to measure electric resistivity. Au/Ti pads for electrodes are sputtered on AZO layer through a stencil mask. The glass mold as shown in Fig. 4(b) is used for the measurement of thermal conductivity because a silicon mold cannot be used due to its high thermal conductivity. A glass mold has many through holes of 10  $\mu\text{m}$  diameter. Thermal conductivity is measured by using the laser flush method. The calculated thermal conductivity of the AZO is taken the thermal conductivity of the glass mold into consideration; however, the heat flow from AZO to the glass mold is disregarded in this report.

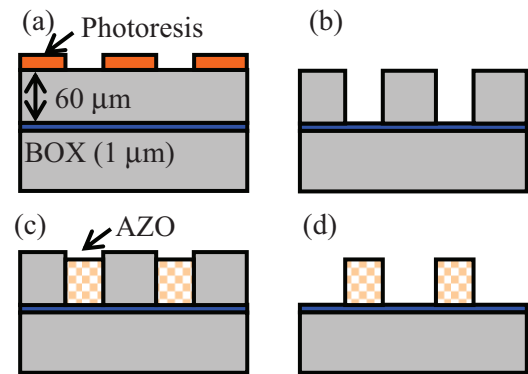


Fig. 3: A fabrication process of microstructures. (a) Patterning. (b) DRIE of Silicon. (c) Deposition of AZO. (d) Etching the silicon mold.

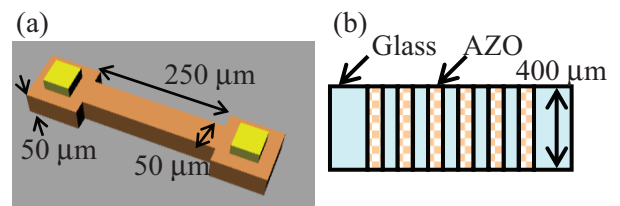


Fig. 4: Test structures. (a) A test structure to measure electric resistivity. (b) A glass mold to measure thermal conductivity.

## DISCUSSION

Figure 5 shows a comparison of deposited AZO films by AD on the flat part of a silicon wafer and in the micromachined mold. The primary size of the powder used is 200 nm. The trench width and depth are 20  $\mu\text{m}$  and 100  $\mu\text{m}$ , respectively. The thickness of the deposited AZO on the flat part is about 60 nm. This thickness is a saturated value and doesn't increase with scan times as shown in Fig. 6. This result corresponds to Akedo's prediction in that it is difficult to obtain thick ZnO layers by AD [9]. The micromachined mold is filled with AZO powder. The filled powder does not appear to form a dense ceramic layer and exist as pressed powder, different from that of powder on a flat surface. It is supposed that the structure is fragile; however, it is not destroyed by megasonic cleaning at 1 MHz.

Figure 7 shows the filled height after mold filling with various powder sizes and trench widths. The sizes of the powder used are 3  $\mu\text{m}$  and 200 nm. The trench depth of the silicon mold is 60  $\mu\text{m}$  and the width changes between 5  $\mu\text{m}$  to 500  $\mu\text{m}$ . Both AZO powder sizes are filled well into the minimum trench with a 5- $\mu\text{m}$ -width, and the filled levels decrease with an increased trench width. The mold filling seems to be effectively achieved with narrow trenches. This is caused when powder injected into wide trenches soon escapes out-of-trench in the same manner as that when injected into flat surfaces. In terms of a comparison with powder size, smaller-diameter powder can fill wider trenches. These results show that the powder of a small size is more suitable for mold filling under this AD condition. Mold filling with powder is achieved effectively between the 5- $\mu\text{m}$ -width and 100- $\mu\text{m}$ -width. There is a possibility that using a smaller powder will lead to both better filling and improved thermoelectric properties by quantum confinement.

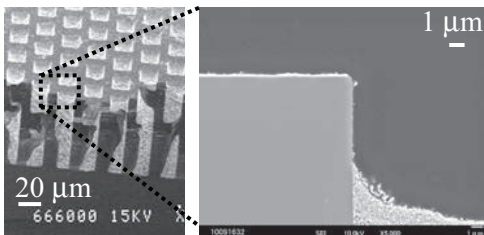


Fig. 5: A Cross-sectional SEM image of mold filling.

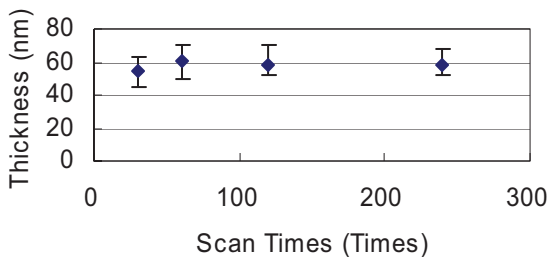


Fig. 6: Deposition thickness on the flat silicon wafer.

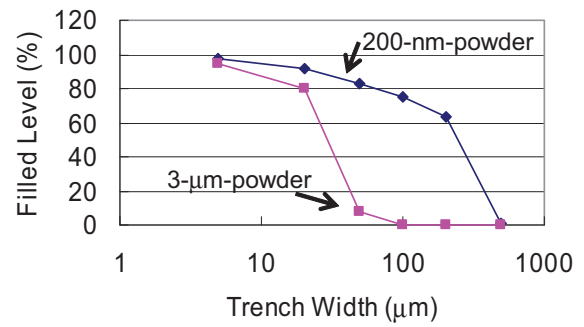


Fig. 7: Filled level of various width trenches.

Figure 8 shows the SEM images of fabricated AZO microstructures with various sizes that are obtained after selective silicon etching. Figure 8(a) shows a 20- $\mu\text{m}$ -square structure that is stably fabricated. Figure 8(b) shows the densest integration at about 2500 pillars/ $\text{mm}^2$ , which has an aspect ratio of 5 at a 10- $\mu\text{m}$ -square-trench. Figure 8(c) shows the smallest structure obtained that has an aspect ratio of 10 at a 5- $\mu\text{m}$ -square trench. These structures often cannot stand alone on the BOX layer. Almost the same shape as the silicon molding is obtained in all sizes. This reveals that this method can be used to form various ceramic structure shapes.

Figure 9 shows cross-sectional SEM images of fabricated micro pillars with a 20- $\mu\text{m}$ -square trench. Figure 9(a) shows a morphology of the as-deposited structure. This is formed by pressed powder with many grain boundaries. Figure 9(b) and 9(c) show the morphologies of the  $\text{N}_2$  annealed structure at 400 degrees C and 1000 degrees C, respectively. We confirmed that the grain boundaries are gradually disappeared with the post-annealing thermal energy.

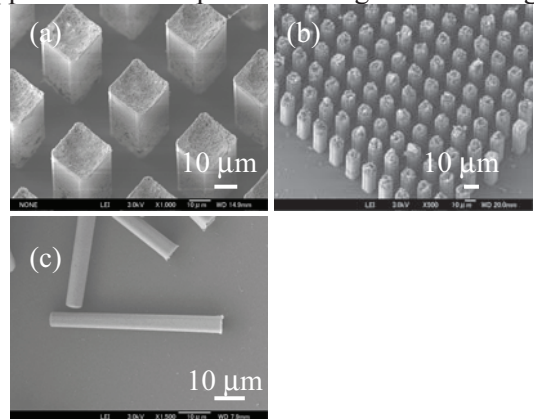


Fig. 8: SEM images of fabricated microstructures.

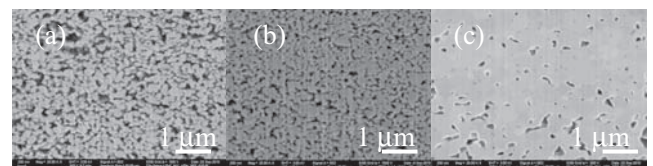


Fig. 9: SEM images of surface morphologies.

Figure 10 shows the I-V characteristics of a fabricated test structure. The electric resistivity of the as-deposited sample is about 2.8k  $\Omega\text{cm}$ . This value is considerably higher than that of bulk AZO and corresponds to pressed powder at about 3 MPa at room temperature. The electric conductivity improves by  $\text{N}_2$  post-annealing. The values after sintering are about 590  $\Omega\text{cm}$  at 400 degrees C and about 60  $\Omega\text{cm}$  at 1000 degrees C. This is considered due to the fact that post-annealing reduces the boundary resistance of powder. Improvement of about 1/50 was obtained. Table 2 shows the calculated thermal conductivities. Note that this result was obtained by using different patterns for electric measurement and by disregarding the heat flow. The measured thermal conductivity of the as-deposited sample is about 0.22 W/(mK), which is about 1/100 of the bulk AZO. This is probably due to heat conduction that was efficiently suppressed with the nanovoids formed in the structure [10]. Post-annealing at 400 degrees C also increases thermal conductivity to 0.37 W/(mK). The point that should be considered is that the amount of change in thermal conductivity by sintering is less than that in the case of electric conductivity. These results imply that post-annealing improves the thermoelectric properties of the filled AZO. This suggests the possibility that optimizing the AD conditions and annealing may lead to higher electric conductivity and lower thermal conductivity.

When the above-mentioned results are compared with the previous work [5], the electric resistivity and thermal conductivity are about four orders higher and two orders lower, respectively. The measured Seebeck coefficient using the glass mold is about -50  $\mu\text{V/K}$  at room temperature, which is almost the same value. We suppose that the fabricated structure has a lower dimensionless figure of merit (ZT) than that of the bulk AZO; however, we anticipate improvement with the optimization of the AD conditions and heat-treatment.

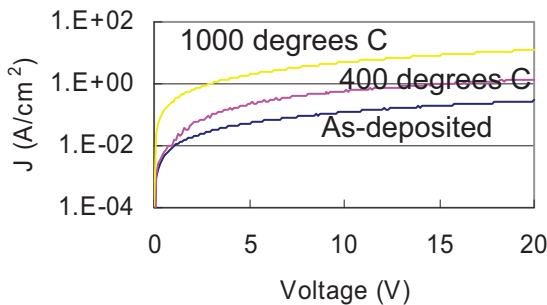


Fig. 10: I-V characteristics of fabricated microstructures.

Table 2: Measured result of thermal conductivities.

| Items                  | Thermal Conductivity |
|------------------------|----------------------|
| As-deposited           | 0.22 [W/(mK)]        |
| Annealed at 400 deg. C | 0.37 [W/(mK)]        |
| Glass mold             | 0.30 [W/(mK)]        |

## CONCLUSION

We have developed a fabrication method that combines AD and a micromachined molding process. We succeeded in forming various AZO microstructures with high-density integration of 2500 pillars/ $\text{mm}^2$  and high-aspect-ratio of 5 at a 10- $\mu\text{m}$ -square-trench on silicon wafers by optimizing powder sizes and trench sizes. The thermoelectric property of the fabricated structure was lower than that of the bulk; however, it was demonstrated that the properties are improved by post-annealing. This suggests that the presented method has the potential for realizing new power MEMS devices having promising geometries.

## REFERENCES

- [1] W. Glatz, S. Muntwyler, C. Hierold 2006 Optimization and fabrication of thick flexible polymer based micro thermoelectric generator *Sensors and Actuators A: Physical*, 132 (2006), pp. 337-345.
- [2] H. Bottner, J. Nurnus, A. Gavrikov, G. Kuhner, M. Jagle, G. Kunzel, D. Eberhard, G. Plescher, A. Schubert, K-H. Schlereth 2004 New thermoelectric components using microsystem technologies *J. Micromech. Syst.*, vol.13 (2004), pp. 414-420.
- [3] A. Chen, D. Madan, M. Koplou, P. K. Wright, J. W. Evans 2009 Dispenser printed thermoelectric energy generators *Technical Digest PowerMEMS 2009* pp. 277-280.
- [4] J-F. Li, S. Tanaka, T. Umeki, S. Sugimoto, M. Esashi, R. Watanabe 2003 Microfabrication of thermoelectric materials by silicon molding process *Sensors and Actuators A: Physical*, 108 (2003), pp. 97-102.
- [5] H. Cheng, X. J. Xu, H. H. Hng, J. Ma 2009 Characterization of Al-doped ZnO thermoelectric materials prepared by RF plasma powder processing and hot press sintering *Ceram. Int.*, 35 (2009), pp. 3067-3072.
- [6] S. Tanaka, S. Sugimoto, J-F. Li, R. Watanabe, M. Esashi 2001 Silicon carbide micro-reaction-sintering using micromachined silicon molds *J. Micromech. Syst.*, vol.10 (2001), pp. 55-61.
- [7] J. Akedo, J. Park, H. Tsuda 2009 Fine patterning of ceramic thick layer on aerosol deposition by lift-off process using photoresist *J. Electroceram*, 22 (2009), pp. 319-326.
- [8] M. Ohtaki, T. Tsubota, K. Eguchi, H. Arai 1996 High-temperature thermoelectric properties of  $(\text{Zn}_{1-x}\text{Al}_x)\text{O}$  *J. Appl. Phys.* 79(1996) pp. 1816-1818.
- [9] J. Akedo ISBN978-4-7813-0017-7 C3054 in Japanese pp. 45-46.
- [10] M. Ohtaki, R. Hayashi 2006 Enhanced Thermoelectric performance of nanostructured ZnO, *Proc. 25th Int. Conf. Thermoelectrics, IEEE*, (2006) pp. 276-279.